Extreme events associated to ENSO in control and scenario GCM simulations

Álvarez-García, F., W. CabosNarváez, I. Pérez-González, M. J. OrtizBeviá
University of Alcalá, Spain
Corresponding autor: franciscoj.alvarez@uah.es

Introduction

On account of their potentially severe socio-economic impact, temperature extremes are a subject of great interest within the field of climate research. This is even more so when there appear to exist indications that global climate change might bring about an intensification of these extreme phenomena. The prediction of these changes, and of the probability of occurrence of extreme episodes themselves, would clearly benefit from a better understanding of how they are affected by relevant climatic signals such as El Niño-Southern Oscillation (ENSO). We are currently investigating these relationships in coupled model data from both control and scenario simulations, in an attempt to elucidate how the impacts of ENSO on the daily data statistics might be modified under global warming conditions. Some results for the GFDL coupled model are presented here.

Data and methodology

We analyze daily maximum and minimum surface temperature and monthly sea surface temperature (SST) data from different simulations with the Geophysical Fluid Dynamics Laboratory (GFDL) coupled model (Delworth *et al.*, 2006). The atmospheric model has a horizontal resolution of 2°×2.5° in latitude and longitude, respectively, and 24 vertical levels. The ocean has a latitudinal resolution of 1°, increased to 1/3° in equatorial regions. The longitudinal resolution is 1°, and there are 50 vertical levels. The sea ice model has the same horizontal resolution as the ocean model. The model runs with a coupling frequency of 2 h., without any flux adjustment.

We examine a control run of 500 years with greenhouse gas (GHG) concentrations held fixed at conditions around 1860, and a climate change simulation of 240 years with concentrations varying as observed between 1861 and 2000, and then following the SRES A2 scenario during the 21st century.

The characteristics of ENSO in both simulations are addressed in the first place. Warm ENSO episodes are identified in the Niño3 Index (average SST anomaly over [150°W-90°W, 5°S-5°N]) when the one-standard-deviation threshold of the time series is crossed. In the case of the scenario simulation, the SST anomalies are previously detrended. The evolution of the tropical Pacific SST anomalies during different episodes is compared by means of a clustering technique that classifies events into groups showing common features; the classification procedure takes into account the spatial correlation between SST anomalies within 15°S and 15°N all along the development of different episodes (Álvarez-García *et al.*, 2006). Once diverse kinds of ENSO events have been detected, their impacts on the daily maximum and minimum temperature data are investigated. Two different stages are considered: the year of development of the episode (hereinafter, year 0) and the year of termination (hereinafter, year +1). We monitor the effects on the daily temperature distribution in terms of the fraction of days per year, for the collection of 'years 0' and 'years +1' associated with the different types of ENSO episodes, when the 90th percentile of the full daily record (computed locally and on a multi-year basis) is surpassed.

Results

A total number of 81 ENSO events are identified in the 500 years of data of the control simulation, while 42 episodes are detected in the 240 years of the climate change run. For both simulations, the clustering results in two classes of ENSO episodes, hereinafter class I and class II, that show similar features in each run. Most of the events are included in these groups, with only about 1/8 of the episodes remaining unclassified in both runs. Class I includes 40 events in the control simulation, and 20 in the climate change simulation. Figures 1a and 1c depict the evolution of SST anomalies averaged between 5°S and 5°N in the Class I composite event. It corresponds to a relatively long warming with traces of eastward propagation along the equator. Class II episodes, of which there are 30 cases in the control run and 17 in the climate change run, are shorter and rather show slightly westward propagation of SST anomalies along the equator as illustrated in Figures 1b and 1d.

Figure 2 depicts the changes in the fraction of days with maximum temperature above the 90th percentile of the full record, associated with each of the ENSO classes, under control and under climate change conditions. These changes are similar in the case of daily minimum temperature, so the corresponding figures are omitted.

The comparison of the control and climate change conditions reveals stronger modification in the impacts of Class II episodes than in the case of Class I events. Areas of cooling (where the fraction of days above the 90th percentile falls below 10%) extend considerably during both year 0 and year +1 of Class II episodes in the climate

change simulation with respect to the control run, and warming in some locations, such as the north-eastern parts of the American continent in year +1, for instance, practically disappears.

In contrast to this, the impacts of the Class I events in the control and in the climate change runs are essentially similar, but for a reduced warming in the eastern equatorial Pacific and smaller extension of cool areas in the extratropical Pacific.

In summary, our study suggests the influence of ENSO on the distribution of daily temperatures thoughout the globe might be affected by climate change, in a mode-dependent way.

Acknowledgments

This work was supported by the project CAM-UAH-2005-059.

References

Álvarez-García F., W. CabosNarváez, and M. J. Ortiz Beviá, 2006: An assessment of differences in ENSO Mechanisms in a Coupled GCM Simulation, *J. Climate*, **19**, 69-87.

Delworth, T. L., A. Rosati, R.J. Stouffer, K. W. Dixon, J. Dunne, K. Findell, P. Ginoux, A. Gnanadesikan, C. T. Gordon, S. M. Griffies, R. Gudgel, M. J. Harrison, I. M. Held, R. S. Hemler, L. W. Horowitz, S. A. Klein, T. R. Knutson, S.-J. Lin, P. C. D. Milly, V. Ramaswamy, M. D. Schwarzkopf, J. J. Sirutis, W. F. Stern, M. J. Spelman, M. Winton, A. T. Wittenberg, B. Wyman, F. Zeng, and R. Zhang, 2006: GFDL's CM2 Global Coupled Climate Models. Part I: Formulation and simulation characteristics. *J. Climate*, **19**, 643-674.

Caption List

Figure 1: Time-longitude diagram of SST anomalies averaged between 5°S and 5°N: a) control run, class I; b) control run, class II; c) climate change run, class I; d) climate change run, class II.

Figure 2: Fraction of days (%) with daily maximum temperature above reference 90th percentile: a) control run, class I-year 0; b) scenario run, class I-year 0; c) control run, class I-year +1; d) scenario run, class I-year +1; e) control run, class II-year 0; f) scenario run, class II-year 0; g) control run, class II-year +1; h) scenario run, class II-year +1.

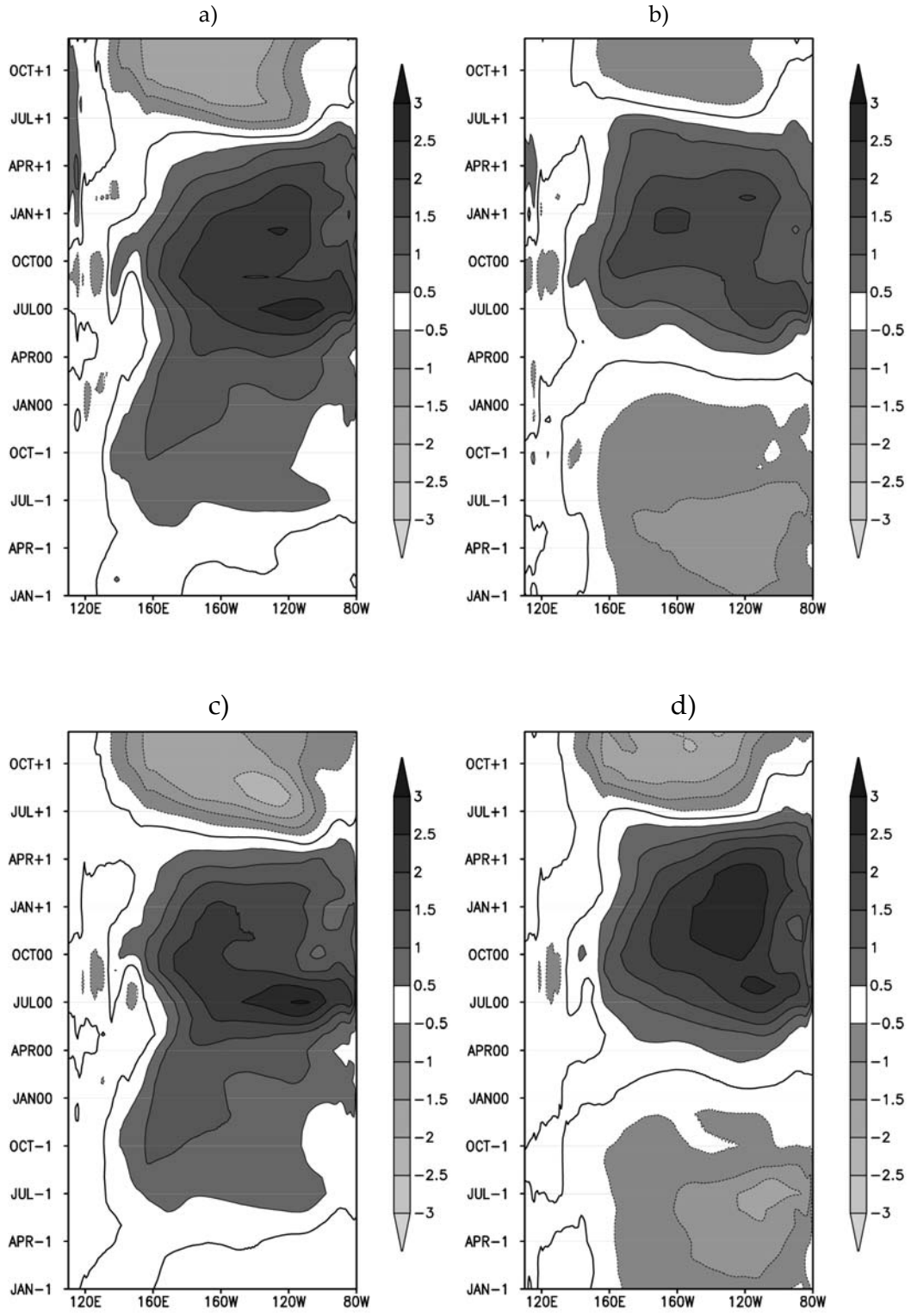

Figure 1: Time-longitude diagram of SST anomalies averaged between 5°S and 5°N: a) control run, class I; b) control run, class II; c) climate change run, class I; d) climate change run, class II.

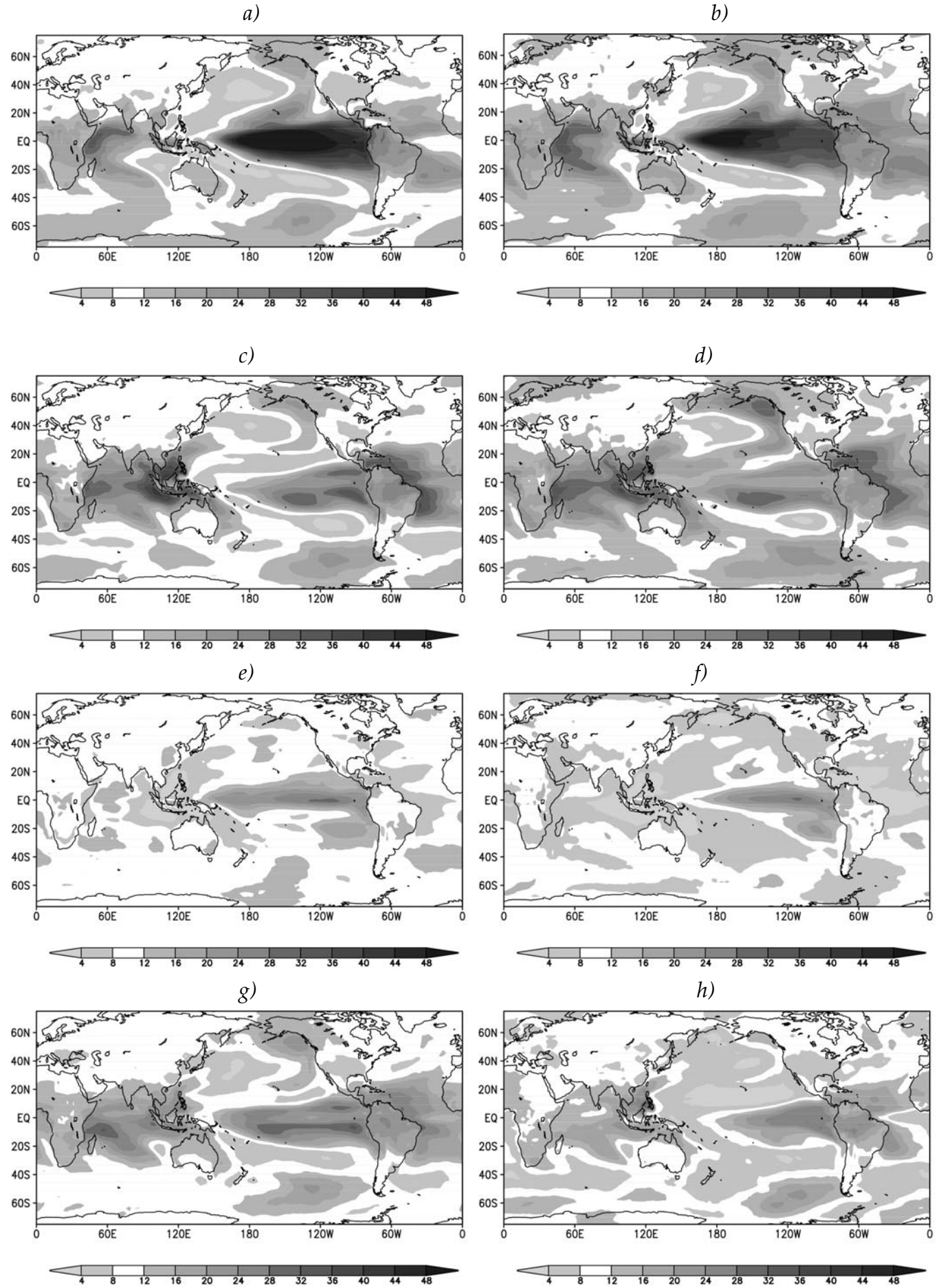

Figure 2: Fraction of days (%) with daily maximum temperature above reference 90th percentile: a) control run, class I-year 0; b) scenario run, class I-year 0; c) control run, class I-year +1; d) scenario run, class I-year +1; e) control run, class II-year 0; f) scenario run, class II-year 0; g) control run, class II-year +1; h) scenario run, class II-year +1.